Diagn Interv Radiol 2016; 22: 22–28

ABDOMINAL IMAGING

PICTORIAL ESSAY

Different forms of iron accumulation in the liver on MRI

İlkay S. İdilman
Deniz Akata
Mustafa Nasuh Özmen
Muşturay Karçaaltıncaba

ABSTRACT

Magnetic resonance imaging (MRI) is a well-established imaging modality to evaluate increased iron deposition in the liver. Both standard liver imaging series with in-phase and out-of-phase T1-weighted sequences for visual detection, as well as advanced T2- and T2*-weighted measurements may be used for mapping the iron concentration. In this article, we describe different forms of liver iron accumulation (diffuse, heterogeneous, multinodular, focal, segmental, intralesional, periportal, and lobar) and hepatic iron sparing (focal, geographic and nodular). Focal iron sparing is characterized by hypointense areas on R2* map and hyperintense areas on T2* map. We also illustrate MRI findings of simultaneous hepatic iron and fat accumulation. Coexistence of iron (siderosis) and fat (steatosis) can make interpretation of in- and out-of-phase T1-weighted images difficult; calculation of proton density fat fraction and R2* maps can characterize abnormal signal changes observed on in- and out-of-phase images. Knowledge of different forms of hepatic iron overload and iron sparing and evaluation of T2* and R2* maps would allow correct diagnosis of iron-associated liver disorders.

Magnetic resonance imaging (MRI) findings of iron overload, particularly in the liver, are well established (1). Hepatic iron overload is abnormal accumulation of iron in hepatocytes, Kupffer cells, or both (2, 3). Hepatic iron overload is commonly associated with hereditary hemochromatosis, transfusion-related iron overload, and chronic hepatopathies (4). MRI is mainly preferred for detection of hepatic iron. However, different forms of iron accumulation and iron sparing can make interpretation of images difficult. Knowledge of different forms of hepatic iron overload and iron sparing, and evaluation of T2* and R2* maps would allow correct diagnosis of iron-associated liver processes. In this article, we aimed to describe different forms of hepatic iron overload (diffuse, heterogeneous, multinodular, focal, hypersiderosis, segmental, intralesional, and periportal) and hepatic iron sparing (focal, geographic and nodular, and periportal) (Table).

Techniques for evaluation of hepatic iron overload

Ultrasonography

Ultrasonography is not a suitable technique for evaluation of hepatic iron overload, as it cannot detect iron deposition (5). However, nonspecific long-term changes caused by hepatic iron overload like cirrhosis, portal hypertension, or hepatocellular carcinoma can be detected by ultrasound.

Computed tomography

Iron overload is presented as increased liver attenuation (72 HU or more) on unenhanced computed tomography (CT) images due to increased absorption of X-rays by iron (6). Associated hepatic steatosis, which is characterized as decreased attenuation on CT may potentially reduce sensitivity, whereas other factors increasing attenuation of hepatic parenchyma like gold storage in liver (7) and amiodarone administration (8) decrease the specificity of this technique. Therefore, CT is not a reliable technique for diagnosis and quantification of iron overload in the liver. However, CT may be of use in some patients unsuited for MRI, or to differentiate high iron content from calcifications, air, or foreign materials such as surgical clips.

Magnetic resonance imaging

Iron causes a local distortion in the magnetic field and results in T1, T2, and T2* shortening. This effect causes signal loss on T2-weighted spin-echo/fast spin-echo and T2*-weighted gradient echo images, and is used for measurement of iron concentration. Iron-induced T2* short-

From the Department of Radiology (M.K. ✉ *musturayk@yahoo.com*), Hacettepe University School of Medicine, Ankara, Turkey.

Received 11 March 2015; revision requested 22 April 2015; revision received 1 June 2015; accepted 1 July 2015.

Published online 2 November 2015.
DOI 10.5152/dir.2015.15094

ening is superior to iron-induced T2 shortening, therefore T2*-weighted images have greater sensitivity to detect iron (9), and are more commonly used for this purpose. It is important to be alert to detect iron overload in the liver, as it is not always clinically evident. In routine abdominal MRI protocols, in- and out-of-phase images, which are generally used for detection of fat, are also helpful in detection of iron. Iron causes signal drop on standard in-phase images, contrary to signal drop effect of fat on out-of-phase. With this principle, many iron quantification methods by MRI depends on gradient echo sequences with T2* weighting, which were acquired with progressively longer echo times.

There are two major methods in quantification of hepatic iron overload, namely, signal intensity ratio methods and relaxometry methods. Signal intensity ratio methods measure the signal intensity of the liver and another tissue or noise and give proportion of these to quantify the liver iron (10, 11), whereas relaxometry methods measure signal intensity of the liver across multiple echo times and calculate T2 or T2* values depending on the performed sequence (12). T2 or T2* values are inversely related with iron concentration. However, R2 or R2* values (1000/T2 or T2*) are directly related to the iron concentration and increase linearly with iron concentration determined by liver biopsy (13). Calculation of R2* and T2* plays an important role in diagnosing the degree of iron overload for planning the treatment with iron chelating agents. A T2* value below 18 ms is accepted as hepatic iron overload (14). A recent study demonstrated that the R2* cutoff value of 147.1 Hz (T2* value of 6.8 ms) discriminates moderate and severe hepatic iron overload from absent and mild hepatic iron overload (15).

Magnetic field strength of the scanner is important for measuring R2 and R2* values as cardiac and liver R2* values measured on 3.0 T is higher than values measured on 1.5 T scanner (16). Higher field strength may be an advantage in detection of tissues containing low iron and when high image resolution is needed. However, higher field strength is more sensitive to magnetic susceptibility artifact, and heavy iron overload in the tissue may cause problem in detection and quantification of iron (17). The software for calculating R2 and R2* maps is not available on all MRI scanners. Apart from these, MRI is a good alternative to biopsy for both diagnosis and treatment monitoring of hepatic iron overload.

Table. Different forms of hepatic iron overload and iron sparing

Hepatic iron overload	Associated conditions
Diffuse siderosis	Hemosiderosis, hemochromatosis
Heterogeneous siderosis	Iron chelation treatment
Focal and segmental siderosis	Infarction
Hypersiderosis	Hemosiderosis
Intralesional siderosis	Regenerative nodule
	Dysplastic nodule
	Hemorrhagic focal liver lesions (hepatic adenoma, hepatocellular carcinoma, choriocarcinoma, melanoma)
Periportal siderosis	Early hemosiderosis
	Iron chelation treatment
Hepatic iron sparing	
Focal nodular and geographic iron sparing	Hemosiderosis
Periportal iron sparing	Periportal cavernomatous transformation

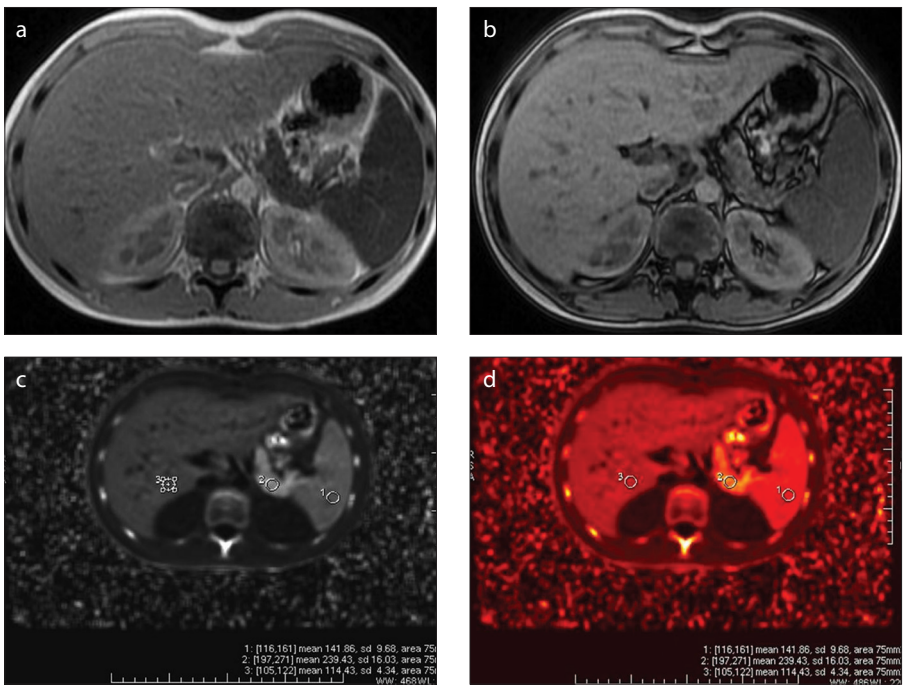

Figure 1. a–d. Diffuse siderosis in a patient with thalassemia major. There is signal drop on in-phase image **(a)** relative to out-of-phase image **(b)**. R2* measurements on R2* map **(c)** and colored R2* map **(d)** demonstrate iron overload in the liver, spleen, and pancreas.

Main points

- Hepatic iron overload can be diagnosed by in- and out-of-phase sequence and T2* and R2* maps.
- MRI is preferred for detection and quantification of hepatic iron.
- Knowledge of different forms of hepatic iron overload and iron sparing would allow correct diagnosis of atypical lesions in hemosiderosis.
- We describe new forms such as hypersiderosis and periportal iron sparing.

Hepatic iron overload

Iron homeostasis depends on the balance between daily gains (intestinal absorption, reuse from old erythrocytes) and losses (epithelial desquamation, menstruation). This balance is crucial, because there is no effective way for excretion of iron from the body (18, 19). There are two distinct etiologic causes of iron overload; inherited or primary iron overload and secondary iron overload

syndromes. Primary iron overload (i.e., hereditary hemochromatosis) is an autosomal recessive disorder in which a defective protein causes increased intestinal absorption of iron from small intestine at 5–10 times the normal rate (20). Secondary iron overload syndromes include iron-loading anemias (i.e., thalassemia, sideroblastic anemia, sickle cell disease, chronic hemolytic anemia, aplastic anemia, pyruvate kinase deficiency), chronic liver diseases (i.e., hepatitis C infection, nonalcoholic fatty liver disease, alcoholic fatty liver disease), and iatrogenic (i.e., red blood cell transfusion, long-term hemodialysis) and miscellaneous causes.

Excess iron primarily accumulates in parenchymal cells, particularly in the liver, pancreas, heart, endocrine glands like thyroid and pituitary, and synovium in primary iron overload. However, in secondary iron overload, iron accumulates in reticuloendothelial system (spleen, Kupffer cells, bone marrow, and lymph nodes). Iron also accumulates in hepatocytes and other parenchymal cells after saturation of reticuloendothelial cells, in secondary iron overload. Detection and quantification of hepatic iron overload is important for both primary and secondary iron overload syndromes. In primary iron overload, liver iron content gives information about the risk for hepatic complications such as fibrosis and cirrhosis (4, 21, 22). In iron-loading anemias, liver iron content provides information about total body iron (23), thus quantification of liver iron content helps to monitor these patients and the treatment (2). Liver biopsy is the current reference standard for detection and quantification of iron overload. There are two main limitations of liver biopsy. First, the invasiveness, for which MRI is a good alternative particularly when repetitive/follow-up measurements are needed for treatment monitoring. Second, the sampling error, for which MRI might even be of benefit to determine the best location for biopsy, since hepatic iron overload can have various distributions, as illustrated in this article (4, 24, 25). Therefore hepatic iron accumulation detection, quantification, and follow-up evaluation after treatment depend on imaging methods, especially MRI as described in the previous section.

Hepatic iron overload can be in the form of diffuse, heterogeneous, segmental, focal, hypersiderosis, intralesional siderosis, and periportal siderosis.

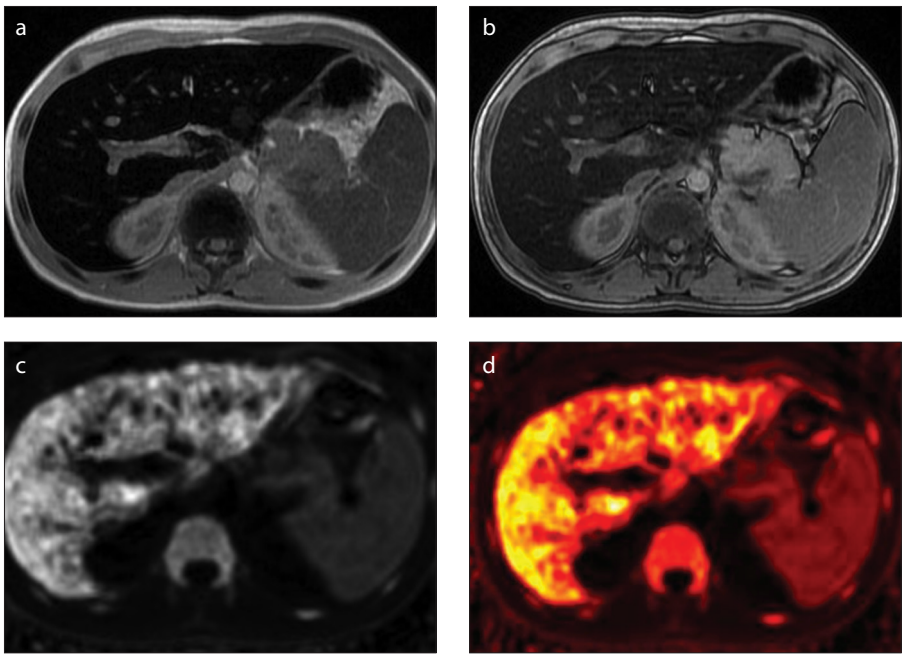

Figure 2. a–d. In-phase **(a)**, out-of-phase **(b)**, R2* map **(c)**, and colored R2* map **(d)** images of a patient with thalassemia major, who is under iron chelation treatment. Heterogeneous siderosis is obvious, especially on R2* map images.

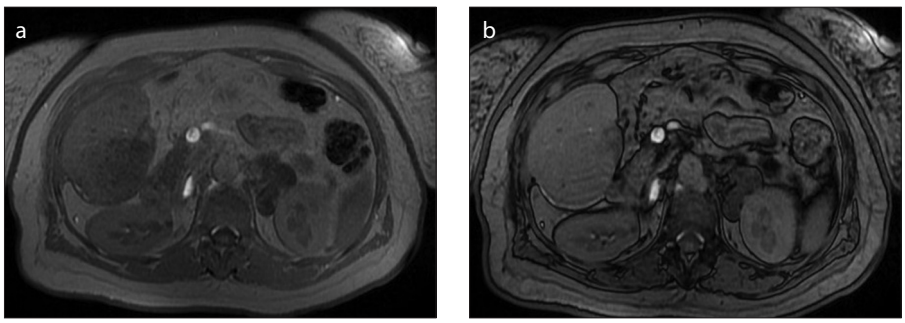

Figure 3. a, b. Focal iron accumulation in segment 6 is seen in a patient with segmental portal vein thrombosis (not shown in the images). There is a signal drop on in-phase image **(a)** compared with out-of-phase image **(b)**.

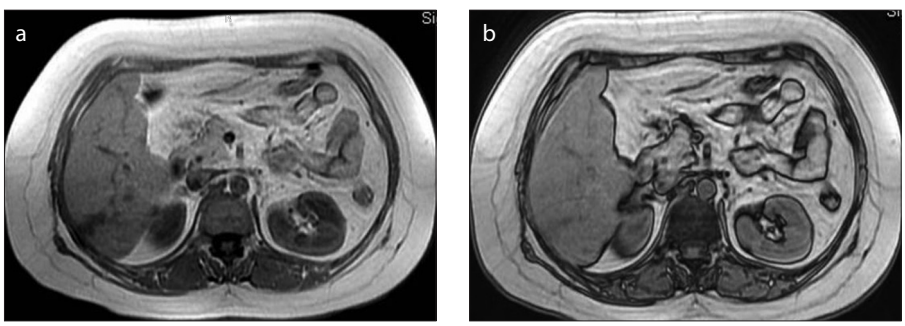

Figure 4. a, b. Focal wedge-shaped iron accumulation in segment 6 is seen in a patient with breast carcinoma most likely due to chemotherapy-related infarction at this location. Note signal drop on in-phase image **(a)** compared with out-of-phase image **(b)**.

Diffuse siderosis

Both primary and secondary iron overload can lead to diffuse hepatic iron overload. However, diffuse siderosis is mostly observed in patients receiving multiple blood transfusions. There is a linear correlation between liver iron concentration and R2* value (1/T2*) (Fig. 1).

Heterogeneous siderosis

Hepatic iron accumulation can be heterogeneous across the liver (26–29). However, this heterogeneity is generally not realized in visual assessment of conventional magnetic

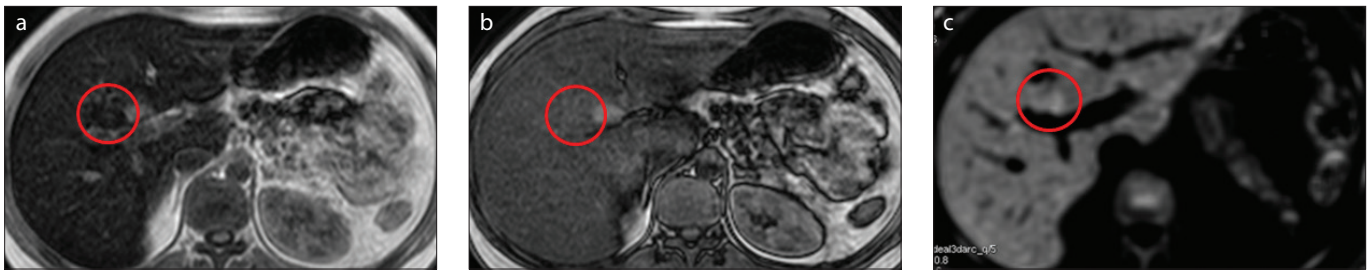

Figure 5. a–c. In-phase **(a)**, out-of-phase **(b)**, and R2* map **(c)** images of a patient with siderosis. A focal hypointense area in segment 4 (within the circle) shows more signal drop than rest of the liver on in-phase image compared to out-of-phase image. This area is also seen hyperintense on R2* map (within the circle), which is consistent with hypersiderosis in a siderotic liver.

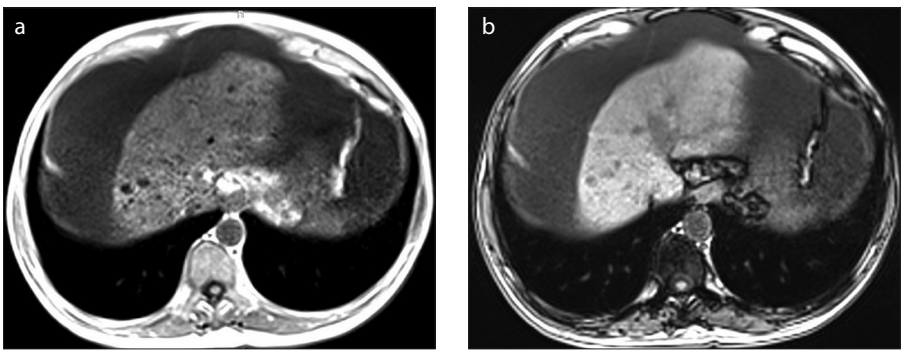

Figure 6. a, b. In-phase **(a)** and out-of-phase **(b)** images demonstrate multiple siderotic nodules in a patient with cirrhosis appearing as hypointense nodules on in-phase images.

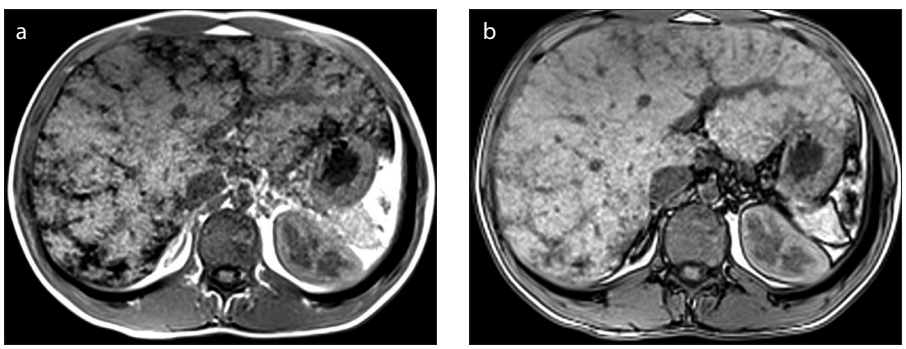

Figure 7. a, b. Periportal signal drop on in-phase image **(a)** compared with out-of-phase image **(b)** in the periportal area due to periportal iron accumulation in a patient with thalassemia major.

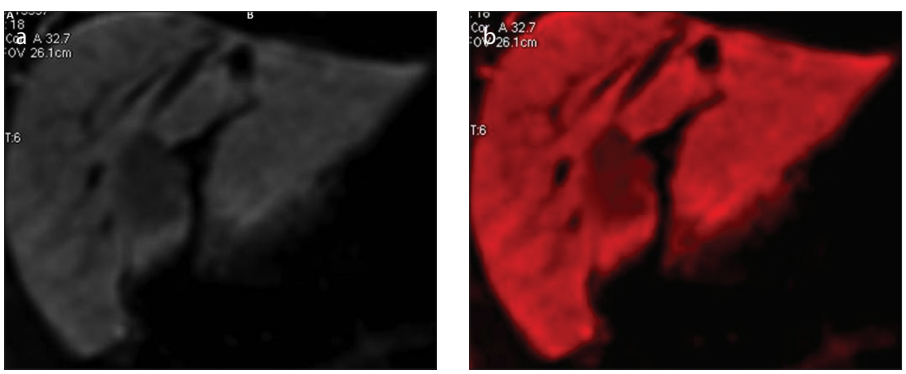

Figure 8. a, b. Focal geographic iron sparing in a patient with aplastic anemia. There is a geographic hypointense area in segment 4 on coronal R2* map **(a)** and colored R2* map **(b)** images.

resonance images. In some cases, especially patients on treatment with iron chelating agents, heterogeneous siderosis can be seen on R2* maps as a treatment response (Fig. 2).

Focal and segmental siderosis

The main distribution of iron to liver is through the portal vein. Situations like thrombosis, compression, or shunting of portal vein that decrease portal venous flow result in unequal iron deposition in different segments. Segmental siderosis was defined as segmental hypointensity on MRI and was confirmed by liver biopsy as iron deposition in previous studies (30–32).

Focal iron accumulation can be seen in liver due to altered or absent perfusion (Fig. 3). We observed areas of focal siderosis in patients who received chemotherapy. Focal iron deposition can be amorphous nodular in shape. These areas demonstrate focal signal drop on in-phase images compared with out-of-phase images (Fig. 4).

Hypersiderosis

Hypersiderosis is seen as an area containing more iron compared with the rest of the liver. Theoretically, hypersiderosis can be seen in areas with third inflow due to aberrant venous drainage. Hypersiderosis appear hyperintense on R2* maps and can be seen in multiple blood transfusions (Fig. 5).

Intralesional siderosis

Iron can accumulate in regenerative or dysplastic nodules, which are referred as "siderotic nodules" in cirrhosis, unrelated to systemic or hepatic iron overload. The detection of siderotic nodule with MRI is not challenging, however, discrimination of dysplastic nodules from regenerative nodules is not feasible (33) (Fig. 6). Development of hepatocellular carcinoma (HCC) in a siderotic nodule has been defined as nodule-in-nodule appearance on T2- or T2*-weighted images, consisting of intermediate-high intensity focus in low-signal intensity siderotic nodule (34, 35). Iron presence can also be shown with MRI in hemorrhagic focal liver lesions like HCCs, hepatic adenomas (36), and some metastatic lesions like choriocarcinoma (37) and melanoma (38).

Periportal siderosis

Excess iron due to increased intestinal absorption initially accumulates in the peri-

portal hepatocytes (39). Therefore, periportal siderosis can be observed in early phases of hepatic iron overload or after chelation treatment (Fig. 7).

Focal hepatic iron sparing in siderotic liver

Iron sparing refers to areas of liver with less iron than surrounding parenchyma, similar to fat sparing in the liver.

Focal nodular and geographic iron sparing

Focal iron sparing can be seen in patients with hepatic iron overload due to hemosiderosis, usually in segment 4. Location of focal iron sparing can match with usual areas of focal fat accumulation and focal fat sparing. Signal abnormalities in these areas most likely result from the third inflow from aberrant venous drainage into the liver. Most common aberrant venous drainage occurs from Sappey veins, right gastric vein, and left gastric vein. Focal iron sparing can be geographic or nodular in shape (Figs. 8, 9). Nodular forms may mimic a lesion (40).

Tumor cells of HCCs secondary to hepatic iron overload-induced cirrhosis don't contain iron (41). In this situation, HCC can also be detected as focal nodular iron sparing.

Periportal iron sparing

Periportal fat accumulation has been described before (39), but we could not find a case with periportal iron sparing in the literature. We observed periportal iron sparing in a patient with periportal cavernomatous transformation and hemosiderosis related to myelodysplastic syndrome (Fig. 10). The possible mechanism of periportal sparing is normal perfusion in the vicinity of periportal space and caudate lobe. Hypertrophy of the caudate lobe supports this mechanism. Therefore, after the administration of iron chelating agent deferoxamine, iron was cleared only from the areas with normal perfusion.

Iron and fat coexistence

There can be coexisting hepatic iron overload and fat accumulation. In previous studies, it was shown that up to 40% of patients with nonalcoholic fatty liver disease have iron overload (42, 43). On the other hand, coexistence of steatosis in patients with primary iron overload was shown to accelerate liver injury (44). In such circumstances, in- and out-of-phase images can cause diagnostic confusion and both detection and quantification of iron and fat become difficult, especially in conventional MRI. However, quantification of both fat and iron is feasible with recent methods that calculate R2* and proton density fat fraction, simultaneously (45). This approach can help to clarify coexistence of siderosis and steatosis and confusing patterns of fat and iron accumulation (40) (Fig. 11).

Conclusion

There are different forms of iron accumulation and sparing in the liver, which can be a result of normal, variant, or abnormal perfusion changes. Recent MRI techniques for hepatic iron detection and quantification can enable better understanding of hepatic iron overload and iron sparing, and may prevent misdiagnosis of focal signal changes related to varying degrees of iron content in patients with siderosis.

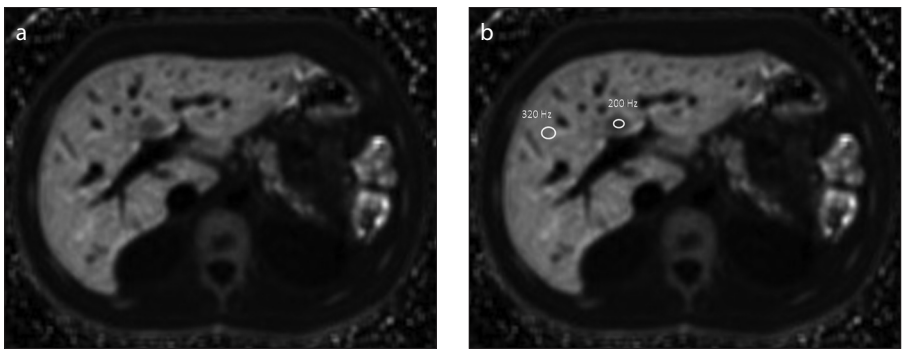

Figure 9. a, b. Focal nodular iron sparing in a patient with thalassemia major. There is a nodular hypointense area in segment 4 on axial R2* map **(a)**. We observed a lower R2* value (200 Hz) in this area compared with the rest of the liver (320 Hz) **(b)**.

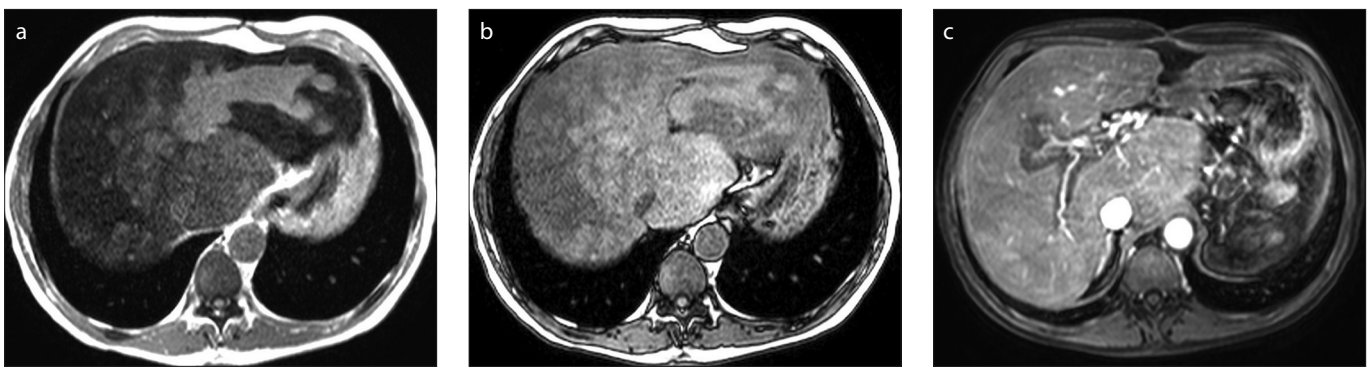

Figure 10. a–c. Periportal iron sparing in a patient with periportal cavernomatous transformation and hemosiderosis related to myelodysplastic syndrome. On in-phase image **(a)** there is a signal drop in liver parenchyma compared with out-of-phase image **(b)** sparing left periportal area. Postcontrast image **(c)** demonstrates chronic thrombosis of portal vein.

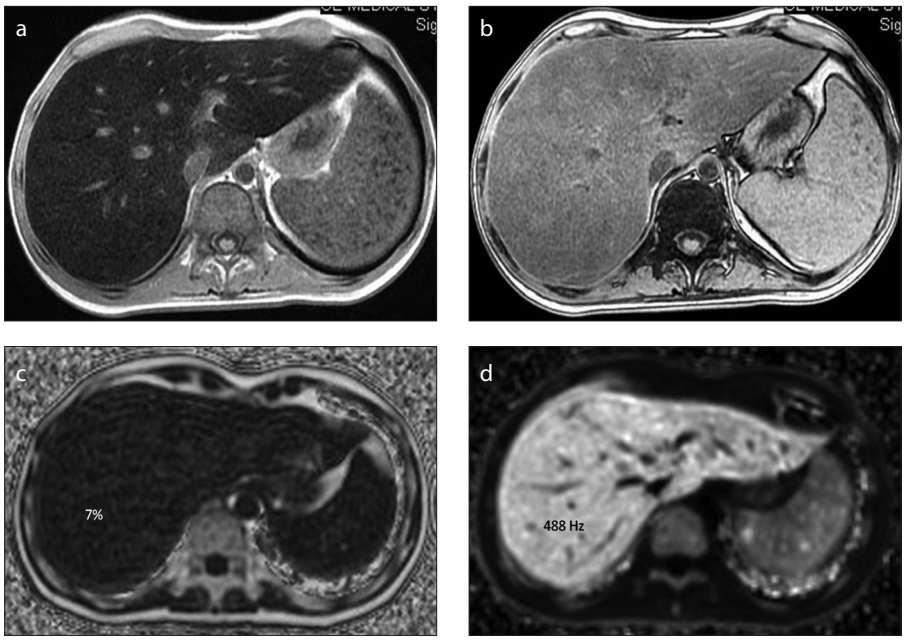

Figure 11. a–d. MRI of a patient with lymphoma show signal drop on in-phase image **(a)** relative to out-of-phase image **(b)** consistent with diffuse siderosis. However, measurements from proton density fat fraction map **(c)** and R2* map **(d)** show coexistence of mild steatosis (7%) and severe siderosis.

Acknowledgements

Muşturay Karçaaltıncaba has been supported by the Turkish Academy of Sciences (TUBA), in the framework of the Young Scientist Award Program (EA-TUBA-GEBIP/2011).

Conflict of interest disclosure

The authors declared no conflicts of interest.

References

1. Queiroz-Andrade M, Blasbalg R, Ortega CD, et al. MR imaging findings of iron overload. Radiographics 2009; 29:1575–1589. [CrossRef]
2. Brittenham GM, Cohen AR, McLaren CE, et al. Hepatic iron stores and plasma ferritin concentration in patients with sickle cell anemia and thalassemia major. Am J Hematol 1993; 42:81–85. [CrossRef]
3. St Pierre TG, Clark PR, Chua-Anusorn W. Single spin-echo proton transverse relaxometry of iron loaded liver. NMR Biomed 2004; 17:446–458. [CrossRef]
4. Adams P, Brissot P, Powell LW. EASL International Consensus Conference on Haemochromatosis. J Hepatol 2000; 33:485–504. [CrossRef]
5. Matheson JS, Paul-Murphy J, O'Brien RT, Steinberg H. Quantitative ultrasound, magnetic resonance imaging, and histologic image analysis of hepatic iron accumulation in pigeons (Columbia livia). J Zoo Wildl Med 2007; 38:222–230. [CrossRef]
6. Guyader D, Gandon Y, Deugnier Y, et al. Evaluation of computed tomography in the assessment of liver iron overload: a study of 46 cases of idiopathic hemochromatosis. Gastroenterology 1989; 97:737–743.
7. De Maria M, De Simone G, Laconi A, Mercadante G, Pavone P, Rossi P. Gold storage in the liver: appearance on CT scans. Radiology 1986; 159:355–356. [CrossRef]
8. Goldman IS, Winkler ML, Raper SE, et al. Increased hepatic density and phospholipidosis due to amiodarone. AJR Am J Roentgenol 1985; 144:541–546. [CrossRef]
9. Li TQ, Aisen AM, Hindmarsh T. Assessment of hepatic iron content using magnetic resonance imaging. Acta Radiol 2004; 45:119–129. [CrossRef]
10. Bonkovsky HL, Rubin RB, Cable EE, Davidoff A, Rijcken TH, Stark DD. Hepatic iron concentration: noninvasive estimation by means of MR imaging techniques. Radiology 1999; 212:227–234. [CrossRef]
11. Gandon Y, Guyader D, Heautot JF, et al. Hemochromatosis: diagnosis and quantification of liver iron with gradient-echo MR imaging. Radiology 1994; 193:533–538. [CrossRef]
12. Alexopoulou E, Stripeli F, Baras P, et al. R2 relaxometry with MRI for the quantification of tissue iron overload in beta-thalassemic patients. J Magn Reson Imaging 2006; 23:163–170. [CrossRef]
13. Wood JC, Ghugre N. Magnetic resonance imaging assessment of excess iron in thalassemia, sickle cell disease and other iron overload diseases. Hemoglobin 2008; 32:85–96. [CrossRef]
14. Westwood M, Anderson LJ, Firmin DN, et al. A single breath-hold multiecho T2* cardiovascular magnetic resonance technique for diagnosis of myocardial iron overload. J Magn Reson Imaging 2003; 18:33–39. [CrossRef]
15. Galimberti S, Trombini P, Bernasconi DP, et al. Simultaneous liver iron and fat measures by magnetic resonance imaging in patients with hyperferritinemia. Scand J Gastroenterol 2015; 29:1–10. [CrossRef]
16. Storey P, Thompson AA, Carqueville CL, Wood JC, de Freitas RA, Rigsby CK. R2* imaging of transfusional iron burden at 3T and comparison with 1.5T. J Magn Reson Imaging 2007; 25:540–547. [CrossRef]
17. Wood JC. Magnetic resonance imaging measurement of iron overload. Curr Opin Hematol 2007; 14:183–190. [CrossRef]
18. Andrews NC. Disorders of iron metabolism. N Engl J Med 1999; 341:1986–1995. [CrossRef]
19. Siah CW, Ombiga J, Adams LA, Trinder D, Olynyk JK. Normal iron metabolism and the pathophysiology of iron overload disorders. Clin Biochem Rev 2006; 27:5–16.
20. Pietrangelo A. Hereditary hemochromatosis--a new look at an old disease. N Engl J Med 2004; 350:2383–2397. [CrossRef]
21. Bassett ML, Halliday JW, Powell LW. Value of hepatic iron measurements in early hemochromatosis and determination of the critical iron level associated with fibrosis. Hepatology 1986; 6:24–29. [CrossRef]
22. Adams PC, Deugnier Y, Moirand R, Brissot P. The relationship between iron overload, clinical symptoms, and age in 410 patients with genetic hemochromatosis. Hepatology 1997; 25:162–166. [CrossRef]
23. Angelucci E, Brittenham GM, McLaren CE, et al. Hepatic iron concentration and total body iron stores in thalassemia major. N Engl J Med 2000; 343:327–331. [CrossRef]
24. Brissot P, Bourel M, Herry D, et al. Assessment of liver iron content in 271 patients: a reevaluation of direct and indirect methods. Gastroenterology 1981; 80:557–565.
25. Alústiza JM, Artetxe J, Castiella A, et al. MR quantification of hepatic iron concentration. Radiology 2004; 230:479–484. [CrossRef]
26. Ambu R, Crisponi G, Sciot R, et al. Uneven hepatic iron and phosphorus distribution in beta-thalassemia. J Hepatol 1995; 23:544–549. [CrossRef]
27. Crisponi G, Ambu R, Cristiani F, et al. Does iron concentration in a liver needle biopsy accurately reflect hepatic iron burden in beta-thalassemia? Clin Chem 2000; 46:1185–1188.
28. Emond MJ, Bronner MP, Carlson TH, et al. Quantitative study of the variability of hepatic iron concentrations. Clin Chem 1999; 45:340–346.
29. Villeneuve JP, Bilodeau M, Lepage R, et al. Variability in hepatic iron concentration measurement from needle-biopsy specimens. J Hepatol 1996; 25:172–177. [CrossRef]
30. Murphy FB, Bernardino ME. MR imaging of focal hemochromatosis. J Comput Assist Tomogr 1986; 10:1044–1046. [CrossRef]
31. Kawamori Y, Matsui O, Kitagawa K, et al. Segmental hepatic iron deposition due to peripheral portal vein tumor thrombus: MR features. J Comput Assist Tomogr 1991; 15:1042–1044. [CrossRef]
32. Kadoya M, Matsui O, Kitagawa K, et al. Segmental iron deposition in the liver due to decreased intrahepatic portal perfusion: findings at MR imaging. Radiology 1994; 193:671–676. [CrossRef]
33. Krinsky GA, Lee VS, Nguyen MT, et al. Siderotic nodules at MR imaging: regenerative or dysplastic? J Comput Assist Tomogr 2000; 24:773–776. [CrossRef]
34. Terada T, Kadoya M, Nakanuma Y, Matsui O. Iron-accumulating adenomatous hyperplastic nodule with malignant foci in the cirrhotic liver. Histopathologic, quantitative iron, and magnetic resonance imaging in vitro studies. Cancer 1990; 65:1994–2000. [CrossRef]
35. Mitchell DG, Rubin R, Siegelman ES, Burk DL Jr, Rifkin MD. Hepatocellular carcinoma within siderotic regenerative nodules: appearance as a nodule within a nodule on MR images. Radiology 1991; 178:101–103. [CrossRef]
36. Grazioli L, Federle MP, Brancatelli G, Ichikawa T, Olivetti L, Blachar A. Hepatic adenomas: imaging and pathologic findings. Radiographics 2001; 21:877–892. [CrossRef]

37. Moon WK, Kim WS, Kim IO, et al. Hepatic choriocarcinoma in a neonate: MR appearance. J Comput Assist Tomogr 1993; 17:653–655. [CrossRef]
38. Premkumar A, Sanders L, Marincola F, Feuerstein I, Concepcion R, Schwartzentruber D. Visceral metastases from melanoma: findings on MR imaging. AJR Am J Roentgenol 1992; 158:293–298. [CrossRef]
39. Ghugre NR, Coates TD, Nelson MD, Wood JC. Mechanisms of tissue-iron relaxivity: nuclear magnetic resonance studies of human liver biopsy specimens. Magn Reson Med 2005; 54:1185–1193. [CrossRef]
40. Karcaaltincaba M, Idilman I, Celik A. Focal sparing of iron and fat in liver tissue in patients with hemosiderosis: diagnosis with combination of R2* relaxometry and proton density fat fraction calculation by MRI. Diagn Interv Radiol 2011; 17:323–327.
41. Terada T, Nakanuma Y. Iron-negative foci in siderotic macroregenerative nodules in human cirrhotic liver. A marker of incipient neoplastic lesions. Arch Pathol Lab Med1989; 113:916–920.
42. George DK, Goldwurm S, MacDonald GA, et al. Increased hepatic iron concentration in nonalcoholic steatohepatitis is associated with increased fibrosis. Gastroenterology 1998; 114:311–318. [CrossRef]
43. Moirand R, Mortaji AM, Loreal O, Paillard F, Brissot P, Deugnier Y. A new syndrome of liver iron overload with normal transferrin saturation. Lancet 1997; 349:95–97. [CrossRef]
44. Powell EE, Ali A, Clouston AD, et al. Steatosis is a cofactor in liver injury in hemochromatosis. Gastroenterology 2005; 129:1937–1943. [CrossRef]
45. Yu H, McKenzie CA, Shimakawa A, et al. Multiecho reconstruction for simultaneous water-fat decomposition and T2* estimation. J Magn Reson Imaging 2007; 26:1153–1161. [CrossRef]